Bulk and surface nanoscale hole density inhomogeneity in $HgBa_2CuO_{4+\delta}$ and $Bi_2Sr_2CaCu_2O_{8+\delta}$ cuprates

Wei Chen,[1] Giniyat Khaliullin,[2] and Oleg P. Sushkov[1]
[1]*School of Physics, University of New South Wales, Sydney 2052, Australia*
[2]*Max-Planck-Institut für Festkörperforschung, Heisenbergstrasse 1, D-70569 Stuttgart, Germany*
(Received 26 October 2010; published 24 February 2011)

It is well established that the hole density in the prototypical superconductor $La_{2-x}Sr_xCuO_4$ is very inhomogeneous due to Sr-dopant induced disorder. On the other hand, the hole distribution in $HgBa_2CuO_{4+\delta}$ and $Bi_2Sr_2CaCu_2O_{8+\delta}$ doped by interstitial oxygen is believed to be much more uniform. Recent nuclear magnetic resonance measurements indicate, however, that the charge inhomogeneity in $HgBa_2CuO_{4+\delta}$ is close to that in $La_{2-x}Sr_xCuO_4$. Calculations performed in the present paper confirm this observation. We also show that the charge inhomogeneity is most pronounced at the surface layer that can be probed by scanning tunneling microscope. Our simulations demonstrate that, despite having similar amplitudes of charge inhomogeneity, the hole mean free path in $HgBa_2CuO_{4+\delta}$ is substantially longer than that in $La_{2-x}Sr_xCuO_4$. The screening of the Coulomb repulsion in $HgBa_2CuO_{4+\delta}$ is also stronger. These two reasons might explain the difference in the superconducting critical temperatures between these two compounds.

DOI: 10.1103/PhysRevB.83.064514 PACS number(s): 74.62.En

I. INTRODUCTION

The nanoscale electronic disorder is a long standing problem in the physics of cuprates. This problem has many aspects, among which the most important one is the influence of disorder on critical temperature T_c. Since the energy scale associated with the pairing mechanism in the CuO_2 plane is believed to be universal, different out-of-plane defects are expected to influence T_c differently.[1,2] Another important aspect is the nanoscale inhomogeneity of the local density of states (DOS) measured by the scanning tunneling microscope (STM). This effect was mostly studied[3–5] in $Bi_2Sr_2CaCu_2O_{8+\delta}$. In this paper, we address theoretically the problem of the nanoscale charge inhomogeneity in cuprates and a related issue of the hole mean free path. We focus on two single layer families of high-T_c superconductors, $La_{2-x}Sr_xCuO_4$ and $HgBa_2CuO_{4+\delta}$, in which the density inhomogeneity has been quantified by nuclear quadrupole resonance (NQR) experiments.[6,7] We also calculate the charge inhomogeneity in the surface layer of $Bi_2Sr_2CaCu_2O_{8+\delta}$.

The NQR measures the energy splitting of nuclear levels induced by an electric field gradient at the nucleus. A hole in the $3d$ shell of the Cu ion gives a dominant contribution to the field gradient at the Cu nucleus. The Cu NQR frequency in cuprates is therefore very sensitive to the doping level and is directly proportional to the local hole concentration. The contribution of the $3d$ hole to the field gradient is significantly compensated by contributions of holes located at nearby oxygens[8,9] therefore the slope of the NQR frequency versus doping varies among different cuprate families.

It is widely accepted that the hole density distribution within the CuO_2 layer in $La_{2-x}Sr_xCuO_4$ is very nonuniform, as it has been clearly demonstrated by measurements of ^{63}Cu NQR spectra.[6] The observed broad NQR spectrum[6] unambiguously indicates a very inhomogeneous hole density profile in the bulk of the sample. The inhomogeneity is due to the doping mechanism, where Sr substitutions of La ions create an effective Coulomb defect very close to the conducting CuO_2 plane. In a recent paper,[10] we have performed the Hartree-Fock simulation of the charge density distribution in $La_{2-x}Sr_xCuO_4$, which shows a very inhomogeneous charge density profile at the nanometer scale, and reproduces the observed NQR lineshapes.

On the other hand, it is generally believed that hole density distribution in compounds doped by interstitial oxygens, such as $HgBa_2CuO_{4+\delta}$ and $Bi_2Sr_2CaCu_2O_{8+\delta}$, is much more uniform than in $La_{2-x}Sr_xCuO_4$. This is because the distance from the interstitial oxygen to the CuO_2 layer is typically larger than the Sr-layer distance in $La_{2-x}Sr_xCuO_4$. However, Cu NQR measurements in the single layer $HgBa_2CuO_{4+\delta}$[7,11] as well as in the bilayer $HgBa_2CaCu_2O_{6+\delta}$[12] show fairly large linewidths comparable to that in $La_{2-x}Sr_xCuO_4$. As it will be demonstrated below, the NQR data imply the same degree of the hole density inhomogeneity in $La_{2-x}Sr_xCuO_4$ and $HgBa_2CuO_{4+\delta}$. We will also show that despite having similar amplitudes of the charge inhomogeneity, the spatial profiles of the density distribution are very different in these two cases: It is much smoother in the oxygen doped $HgBa_2CuO_{4+\delta}$. Consequently, the forward scattering is predominant and the mean free path in $HgBa_2CuO_{4+\delta}$ is substantially longer than that in $La_{2-x}Sr_xCuO_4$. Our simulation also indicates that the screening of the Coulomb repulsion between the charge carriers in $HgBa_2CuO_{4+\delta}$ is stronger. We argue that these two reasons might explain the difference in superconducting critical temperatures between these two compounds.

The nanoscale charge density inhomogeneity in underdoped cuprates is an indirect way to distinguish the large Fermi surface of a normal Fermi liquid and the small Fermi surface of a doped Mott insulator. The calculations in Ref. 10 for $La_{2-x}Sr_xCuO_4$ were based on the small hole pocket Fermi surface, which implies a small number of mobile charge carries. The small number of charge carries results in poor screening[10,13] and hence in the strong charge density inhomogeneity consistent with NQR data. On the other hand, the large Fermi surface implies the large number of mobile charge carriers and a very effective Coulomb screening. In this case

calculations give a very moderate charge inhomogeneity,[14,15] which is too weak to explain the observed NQR linewidths.

Another important point is that the charge inhomogeneity in the surface layer is always stronger than that in the bulk layer. This is because the surface ionic dielectric constant is about two times smaller than that in the bulk.[16] Hence the screening at the surface is weaker and this results in the stronger charge inhomogeneity.

In this paper, we present Hartree-Fock calculations in underdoped cuprates with realistic parameters to simulate the bulk charge distributions in $HgBa_2CuO_{4+\delta}$ and $La_{2-x}Sr_xCuO_4$, and the surface charge distribution in $Bi_2Sr_2CaCu_2O_{8+\delta}$. Our calculation covers from underdoped to optimally doped regimes. We fine-tune theoretical parameters to reproduce experimentally known NQR linewidths.[6,7] This enables us to perform a very accurate comparison of $HgBa_2CuO_{4+\delta}$ and $La_{2-x}Sr_xCuO_4$. We find the charge inhomogeneity of a similar scale in both cases. However, the landscapes of spatial modulations and the hole mean free paths are substantially different. This is due to different positions of the dopant oxygen and the Sr ion relative to the CuO_2 plane. In addition, the dielectric constants in these two compounds are different.

Motivated by STM data[3–5] in $Bi_2Sr_2CaCu_2O_{8+\delta}$, we calculate also the hole density distribution in the surface CuO_2 layer of this compound. The results obtained show a large charge density inhomogeneity comparable to that in the bulk of $HgBa_2CuO_{4+\delta}$. Naturally, the local charge density is highly correlated with the interstitial oxygen positions as has been noticed previously.[13]

The structure of the paper is the following: In Sec. II we formulate the effective model for an isolated CuO_2 layer. Because of the long-range nature of the Coulomb interaction, however, the isolated layer approximation is not sufficient and one has to take into account other layers. The impact of the other layers depends on the way of doping and on structural details, whether this is a single layer or a double layer compound. The single layers $La_{2-x}Sr_xCuO_4$ and $HgBa_2CuO_{4+\delta}$ are considered in Sec. III. In Sec. IV we simulate the charge distribution on the surface of the double layer $Bi_2Sr_2CaCu_2O_{8+\delta}$. We also calculate the correlation function between the local charge density and oxygen dopant positions, and compare the result with the local DOS correlation function measured by STM. Our conclusions are presented in Sec. V.

II. THE EFFECTIVE MODEL FOR A CuO_2 PLANE

We adopt the effective model formulated in Ref. 10 based on the picture of a lightly doped Mott insulator. Throughout the paper we denote the average hole concentration by p and assume $p \ll 1$. The central point is that the number of charge carriers is p instead of $1-p$ as one would expect for a normal Fermi liquid. We consider first an "isolated" CuO_2 layer. The "isolated" means that we disregard the screening effects of the other layers.

To construct a model relevant to cuprates, we first notice that there are the following distinct length scales: (i) The scale of the order of 1–2 lattice spacing where the doped holes are dressed by multiple virtual magnons. (ii) The scale about average separation between Coulomb defects or average separation between holes $\sim 1/\sqrt{p}$. This is the scale of the Coulomb screening. (iii) The scale $r \gg 1/\sqrt{p}$. The Coulomb gap may develop at this scale due to Anderson localization effects.

Regarding the first point, we do not treat the strong correlations explicitly, but instead adopt the effective hole dispersion after quantum fluctuations at short distances are included. To stress this point, we frequently use the term "holon" instead of "hole." It is known that the holon dispersion has minima at momenta $\mathbf{k}_0 = (\pm\pi/2, \pm\pi/2)$, and is approximately isotropic around these points.[17] The bandwidth of the holon is about $2J$, where $J \approx 130$ meV is the superexchange in the t-J model, although we do not directly employ the t-J formalism. Hereafter we set the following energy and distance units:

$$\begin{aligned} J &= 130\ \text{meV} \to 1, \\ a_0 &= 0.38\ \text{nm} \to 1, \end{aligned} \tag{1}$$

where a_0 is the lattice spacing of the CuO_2 plane. To imitate the holon dispersion we consider spinless fermions on a two-dimensional (2D) square lattice. The Hamiltonian reads as follows:

$$H_t = \sum_{\langle ij \rangle} t'' c_i^\dagger c_j, \tag{2}$$

where $c_i^\dagger$ is the holon creation operator at site i and t'' denotes the next-next-nearest-neighbor hopping on the square lattice. The Hamiltonian (2) yields the following dispersion

$$\epsilon_{\mathbf{k}} = 2t''(\cos 2k_x + \cos 2k_y). \tag{3}$$

The dispersion is isotropic around minima at $\mathbf{k}_0 = (\pm\pi/2, \pm\pi/2)$ as shown in Fig. 1. We choose $t'' = 0.25J$ to reproduce the realistic holon band width, about $2J$, as obtained from numerical simulations of the t-J model.[17] An additional argument supporting this value is as follows. Near its minimum the dispersion (2) can be expanded as $\epsilon_{\mathbf{k}} = \approx \text{const} + 4t''|\mathbf{k} - \mathbf{k}_0|^2$, so the holon effective mass is equal to $m^* = \hbar^2/(8a_0^2 t'')$. The value $t'' = 0.25J$ results in the effective mass $m^* \simeq 2m_e$ which is close to the effective mass measured in magnetic quantum oscillation experiments.[18,19] The realistic holon band width and the realistic effective mass justify our choice of $t'' = 0.25J$. We note also that in the original t-J model formalism, there are four holon half-pockets inside the magnetic Brillouin zone, and each pocket has two pseudospins;[17] in the present

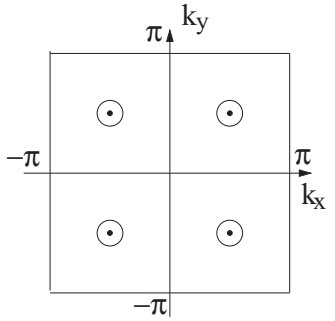

FIG. 1. Dispersion minima of the spinless fermion generated by Hamiltonian (2).

model, we consider four full pockets inside the full Brillouin zone with spinless fermions, hence the number of *charge* degrees of freedom is exactly the same.[20]

Even though the holes are heavily dressed by magnetic fluctuations, their charge is conserved and hence they interact with Coulomb defects via the ordinary Coulomb potential:

$$H_{h-O} = \sum_{l,i} \mathcal{U}_{li} c_i^\dagger c_i, \quad \mathcal{U}_{li} = \frac{-Q}{\sqrt{|\mathbf{R}_l - \mathbf{r}_i|^2 + a_d^2}}, \qquad a_d^2 = a_{\mathrm{ZR}}^2 + \lambda^2. \tag{4}$$

Here $\mathbf{r}_i$ is the position of the holon and $\mathbf{R}_l$ is the in-plane projection of the Coulomb defect (Sr-ion or dopant oxygen) position. The distance from the plane to the defect is λ, and $a_{\mathrm{ZR}} \approx 0.8$ is the size of the Zhang-Rice singlet. (We recall that the energy and distances are given in units of J and a_0, correspondingly.) The dimensionless "charge" $Q \sim 0.5$ depends on the compound, and we discuss its precise values later.

Holon-holon Coulomb interaction is of a similar form

$$H_{\mathrm{int}} = \sum_{ij} U_{ij} c_i^\dagger c_i c_j^\dagger c_j, \quad U_{ij} = \frac{Q}{\sqrt{|\mathbf{r}_i - \mathbf{r}_j|^2 + a_{hh}^2}}, \tag{5}$$

where $a_{hh}^2 \approx 2a_{\mathrm{ZR}}^2 \approx 1$ stands for the combined size of two Zhang-Rice singlets.

The total Hamiltonian

$$H = H_t + H_{h-O} + H_{\mathrm{int}}, \tag{6}$$

describes the in-plane Coulomb problem. Since the Coulomb interaction is not very strong, we solve the many-body problem with the Hamiltonian (6) using the standard Hartree-Fock method. In other words we use the Hartree-Fock decomposition of the Coulomb interaction between holons

$$H_{\mathrm{int}} \to \sum_{ij} U_{ij} \langle c_i^\dagger c_i \rangle c_j^\dagger c_j - \sum_{ij} U_{ij} \langle c_i^\dagger c_j \rangle c_j^\dagger c_i. \tag{7}$$

This can be done for zero as well as for finite temperatures, as it is described in Ref. 10.

The above formulation would solve the Coulomb problem for the "isolated" CuO_2 layer. However, the layer is always embedded in a multilayer structure, and because of the long-range nature of the Coulomb interaction, we have to take into account other layers. Their influence depends on the lattice structure. In the next section, we consider two different families of single layer cuprates.

III. SINGLE LAYER $HgBa_2CuO_{4+\delta}$ AND $La_{2-x}Sr_xCuO_4$ COMPOUNDS. CHARGE DENSITY DISTRIBUTION, NQR LINE SHAPE, DENSITY OF STATES

We treat a particular CuO_2 plane using the Hartree-Fock (HF) method. The role of other CuO_2 planes is to provide screening of the Coulomb interaction in the HF analysis. Since CuO_2 planes have a very high longitudinal polarizability we consider the "other planes" as purely metallic. It has been shown in Ref. 10 that this "metallic approximation" is valid at $p > 1$–2% when the polarizability is sufficiently high. Within this approximation, the HF plane in a single layer compound is sandwiched between two "metallic" sheets, as demonstrated in Fig. 2 for $La_{2-x}Sr_xCuO_4$.

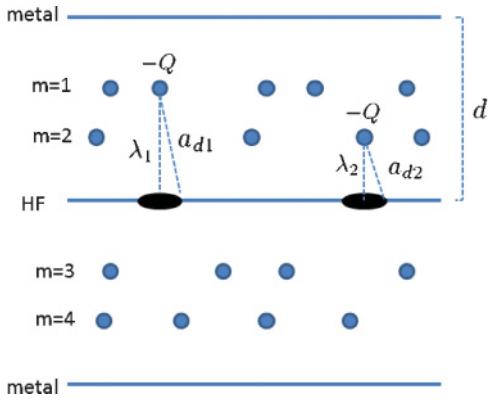

FIG. 2. (Color online) The HF model of $La_{2-x}Sr_xCuO_4$ with four ($m = 1,2,3,4$) layers of Coulomb defects (i.e., doped Sr ions) and with two "metallic" sheets.

A. $La_{2-x}Sr_xCuO_4$

Coulomb defects in $La_{2-x}Sr_xCuO_4$ are created by Sr substitution for La ions. Therefore each defect donates one hole

$$p = x. \tag{8}$$

Given the periodic structure of CuO_2 planes along the c axis, there are two layers of Sr defects between two neighboring CuO_2 planes, as shown in Fig. 2. We mark the defect layers by the index $m = \{1,2,3,4\}$, so the HF CuO_2 plane is under the influence of four layers of Sr defects. The concentration of defects in each defect layer is $x/2$. The planar positions of defects are assumed to be random, and defects are assumed to sit above the center of the Cu plaquette. In addition, in each defect layer we impose a condition that defects never sit next to each other (i.e., the distance between defects is always larger than $\sqrt{2}$). The distance between CuO_2 layers is $d = 1.75$, and the geometric distances to Coulomb defects are $\lambda_1 = \lambda_4 = 1.15$, $\lambda_2 = \lambda_3 = 0.6$. After accounting for the screening by "metallic" planes, the holon interaction with a defect (4) is replaced by

$$\mathcal{U}_{li}^m \to -Q \left(\frac{1}{\sqrt{|\mathbf{R}_l - \mathbf{r}_i|^2 + a_{dm}|^2}} + \sum_{n=1}^{\infty} \frac{(-1)^n}{\sqrt{|\mathbf{R}_l - \mathbf{r}_i|^2 + (2nd + \lambda_m)^2}} + \sum_{n=1}^{\infty} \frac{(-1)^n}{\sqrt{|\mathbf{R}_l - \mathbf{r}_i|^2 + (2nd - \lambda_m)^2}} \right). \tag{9}$$

The summation over n reflects the image method for metallic screening.[10] With values of the distances λ given above, the parameter a_d, defined in Eq. (4), takes the following values: $a_{d1} = a_{d4} = 1.4$ and $a_{d2} = a_{d3} = 1$. The effective charge Q is determined by the dielectric constant of the lattice ϵ_l. In our previous work[10] we used the value $\epsilon_l = 40$ that approximately corresponds to the undoped compound.[21]

This gave a reasonable fit of the NQR lines, but still the widths were about 20–30% larger compared to the experiment. In the present paper, we fine-tune the NQR widths by using ϵ_l as a fitting parameter. Our best fit yields

$$\text{LSCO:} \quad \epsilon_l = 30(1 + 6.25p). \tag{10}$$

Thus the value of ϵ_l depends on doping, $\epsilon_l = 30$ for the undoped compound,[21] and $\epsilon_l = 60$ for the optimally doped compound ($p = 0.16$). The coefficient 6.25 has been obtained by fitting the NQR widths, see below. It is natural to have some doping dependence of the lattice dielectric constant since the lattice dynamics may change locally (get softer) with La $\rightarrow$ Sr substitution. In our dimensionless units, the effective charge Q is

$$Q = \frac{e^2}{\epsilon_l a_0 J} \approx 30/\epsilon_l. \tag{11}$$

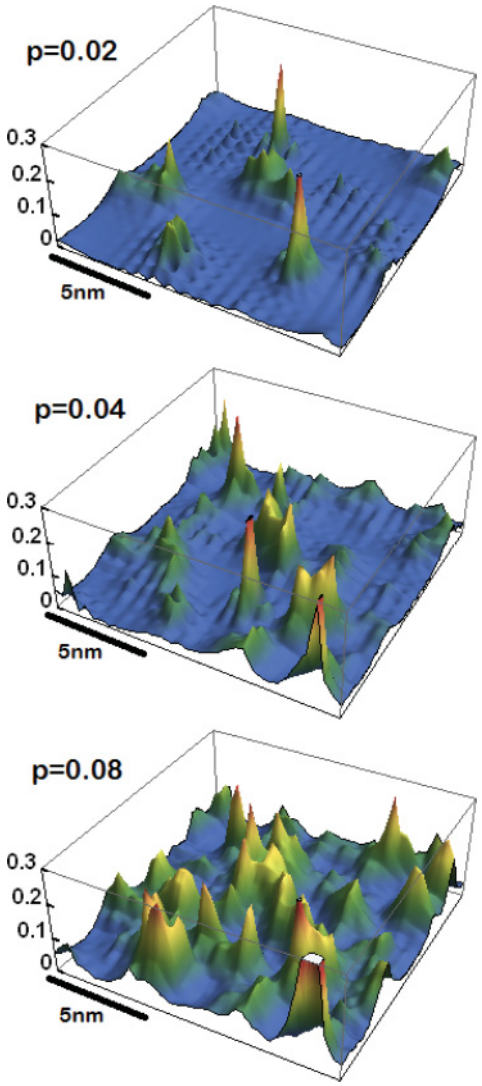

FIG. 3. (Color online) The charge density of mobile holes in $La_{2-x}Sr_xCuO_4$ calculated at zero temperature and different doping levels.

According to the same logic, the Coulomb interaction between holons (5) is replaced by

$$U_{ij} \rightarrow Q\left(\frac{1}{\sqrt{|\mathbf{r}_i - \mathbf{r}_j|^2 + a_{\rm HF}^2}} + \sum_{n=1}^{\infty} \frac{2(-1)^n}{\sqrt{|\mathbf{r}_i - \mathbf{r}_j|^2 + (2nd)^2}}\right). \tag{12}$$

The HF Hamiltonian is diagonalized in a 36×36 cluster. The resulting charge densities for particular realizations of Coulomb defects at different doping levels are shown in Fig. 3. To calculate the NQR spectrum of in-plane ^{63}Cu, we first calculate the hole density distribution averaged over 20 random impurity configurations and then convert the hole density at a site i to the NQR frequency using the following scaling[22]

$$\nu_i = 33 + 19n_i \text{ (MHz)}, \tag{13}$$

which implies that the NQR spectrum is directly related to the charge density distribution. The resulting NQR spectra for zero temperature and for $T = 600$ K are presented in Fig. 4. The theoretical NQR spectra at $T = 600$ K agree very well with the experimental data.[6] Although we are not aware of NQR data at low temperatures, the theoretical spectra at $T = 0$ are shown to demonstrate how the charge density distribution evolves with temperature. It is instructive to present the widths of the charge density distribution.

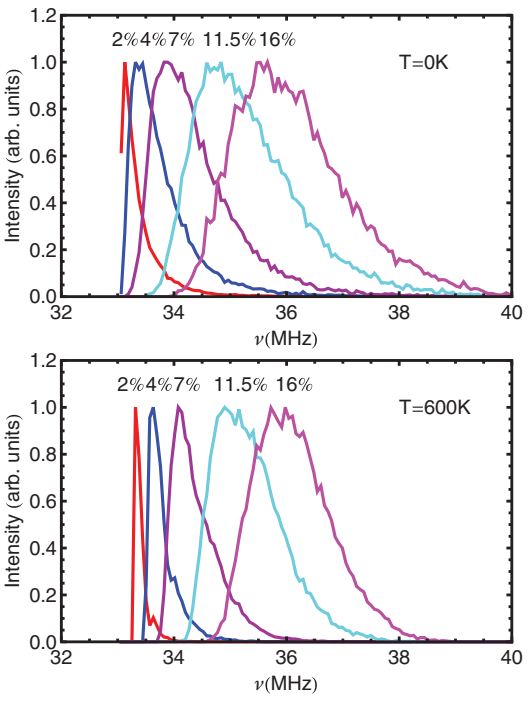

FIG. 4. (Color online) Theoretical NQR spectra for in-plane ^{63}Cu in $La_{2-x}Sr_xCuO_4$ at $T = 0$ and $T = 600$ K and for different doping levels p.

Our simulation yields

$$\text{LSCO}\,at\ p=0.16\text{:}\ \begin{cases}\Gamma_p(T=0)=0.12\\ \Gamma_p(T=600\,\text{K})=0.09,\end{cases}$$
$$\text{LSCO}\,at\ p=0.08\text{:}\ \begin{cases}\Gamma_p(T=0)=0.07\\ \Gamma_p(T=600\,\text{K})=0.05.\end{cases}\qquad(14)$$

In our previous work,[10] we performed similar calculations for $La_{2-x}Sr_xCuO_4$ and demonstrated that the HF calculation reproduces reasonably well the evolution of NQR lineshapes with doping. However, the calculated NQR linewidths were about 20–30% larger compared to the experimental values. The goal of the present calculation is to fit the NQR linewidths quantitatively, using the dielectric constant (10) as a fitting parameter. Based on this fit we accurately quantify the charge inhomogeneity and the hole mean free path as discussed below. We also note that the previous calculation[10] found an additional high frequency hump/shoulder in the NQR line. The hump was due to the strong Coulomb binding of holes to the accidentally clustered Coulomb defects. The binding is very sensitive to the strength of the Coulomb attraction. This binding does not show up in the present calculation because of the larger value of the dielectric constant used, and also due to the fact that we impose here the "nonadjacent" condition for Coulomb defects [see the paragraph before Eq. (9)]. As suggested in Ref. 6, the experimentally observed high frequency hump (the NQR "B line") is most probably due to the direct action of Sr-ion Coulomb potential on the Cu nucleus, which is beyond the scope of the present model.

B. $HgBa_2CuO_{4+\delta}$

Interstitial oxygen ions in $HgBa_2CuO_{4+\delta}$ are located right between two neighboring CuO_2 layers, on top of four adjacent Cu sites.[11] The minimal model for $HgBa_2CuO_{4+\delta}$ is shown in Fig. 5. There is one layer of oxygen defects above the CuO_2 plane and another defect layer below it. The concentration of defects in each defect layer is δ. We assume that each interstitial oxygen donates two holes into the CuO_2 plane, that is,

$$p=2\delta.\qquad(15)$$

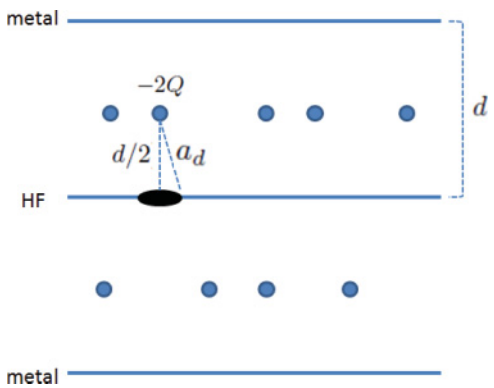

FIG. 5. (Color online) The HF model of $HgBa_2CuO_{4+\delta}$ with two layers of Coulomb defects (interstitial oxygen ions) and two "metallic" sheets.

According to this picture, the holon interaction with a defect, Eq. (4) is replaced by

$$\mathcal{U}_{li}\to -2Q\left(\frac{1}{\sqrt{|\mathbf{R}_l-\mathbf{r}_i|^2+a_d^2}}+\sum_{n=1}^{\infty}\frac{(-1)^n}{\sqrt{|\mathbf{R}_l-\mathbf{r}_i|^2+(2nd+d/2)^2}}+\sum_{n=1}^{\infty}\frac{(-1)^n}{\sqrt{|\mathbf{R}_l-\mathbf{r}_i|^2+(2nd-d/2)^2}}\right).\qquad(16)$$

The interlayer distance in $HgBa_2CuO_{4+\delta}$ is $d=2.5$, and each interstitial oxygen carries "charge" $-2Q$. Taking into account the size of the Zhang-Rice singlet, we have $a_d=\sqrt{a_{\text{ZR}}^2+(d/2)^2}\approx 1.5$. The hole-hole interaction has exactly the same form as that in $La_{2-x}Sr_xCuO_4$, Eq. (12), with the interlayer distance $d=2.5$ and with the value of Q described below. In each defect layer we simulate positions of the defects randomly, and impose again the nonadjacent condition for the defects.

Similar to the procedure in $La_{2-x}Sr_xCuO_4$, we fine-tune the NQR widths using the lattice dielectric constant ϵ_l as a fitting parameter. We find that to fit experimental NQR spectra[7,11] the dielectric constant has to be taken as

$$\epsilon_l=30(1+25p).\qquad(17)$$

Note that the doping dependence of ϵ_l in this case is four times stronger than that in Eq. (10). The stronger dependence is quite natural since it is due to the shift of the interstitial oxygen position in an applied electric field. The shift is significant because the binding of interstitial oxygens in the lattice is weak. In other words, a dopant oxygen brings in new local phonon modes which enhance the dielectric constant. The effective charge Q is determined by the same Eq. (11), with ϵ_l from Eq. (17).

The HF Hamiltonian is diagonalized in a 36×36 cluster. The resulting charge densities for particular realizations of Coulomb defects at different doping levels are shown in Fig. 6. A strong charge inhomogeneity induced by oxygen dopants is apparent. However, density distribution profiles here are much smoother than in $La_{2-x}Sr_xCuO_4$ as one can easily see by comparing Figs. 6 and 3 at the same doping levels.

Now, we address the NQR spectrum of the in-plane ^{63}Cu in $HgBa_2CuO_{4+\delta}$. We first calculate the hole density distribution averaged over 20 random impurity configurations, and then convert the hole density at a site i to the NQR frequency by

$$\nu_i=C+30n_i\ (\text{MHz}),\qquad(18)$$

where C is a doping independent constant. Note that the coefficient 30 MHz in this formula is different from that in Eq. (13). We found the coefficient in Eq. (18) by fitting the NQR-line centers using the experimental data of Ref. 11 (this way is more reliable than using the results of theoretical calculations of electric field gradients[23]). Since NQR data for $HgBa_2CuO_{4+\delta}$ are taken at sufficiently low temperatures, we perform calculations only at $T=0$. Figure 7 shows the theoretical NQR lines by assuming $C=0$ since it is an irrelevant constant shift. The calculations agree well with

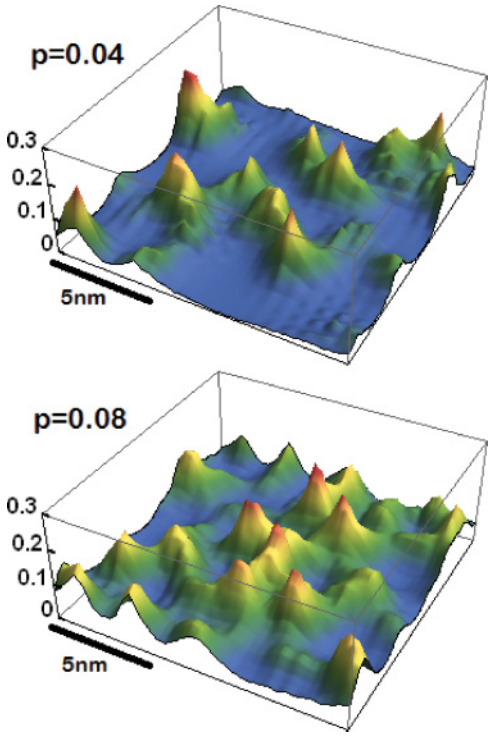

FIG. 6. (Color online) The charge density of mobile holes in $HgBa_2CuO_{4+\delta}$ at zero temperature and at different doping levels.

the experimental data of Refs. 7 and 11. At optimal doping $p = 0.16$, the NQR linewidth in $HgBa_2CuO_{4+\delta}$ is $\Gamma_{\rm NQR} \approx 2.6$ MHz. The widths of the charge density distribution are

$$\begin{aligned} &\text{HBCO } at\ p = 0.16\text{:}\ \ \Gamma_p(T = 0) = 0.09, \\ &\text{HBCO } at\ p = 0.08\text{:}\ \ \Gamma_p(T = 0) = 0.08. \end{aligned} \tag{19}$$

Comparing with the corresponding values for $La_{2-x}Sr_xCuO_4$ in Eq. (14), we see that at zero temperature the amplitudes of charge inhomogeneities in $HgBa_2CuO_{4+\delta}$ and in $La_{2-x}Sr_xCuO_4$ are quite similar. At optimal doping $p = 0.16$, the amplitude of charge inhomogeneity in $HgBa_2CuO_{4+\delta}$ is only by 30% smaller than that in $La_{2-x}Sr_xCuO_4$.

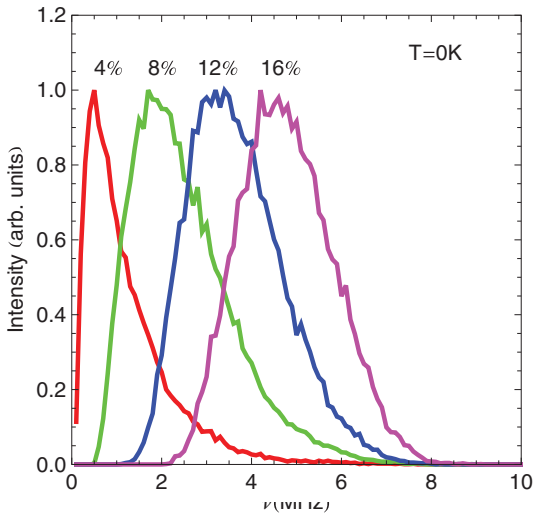

FIG. 7. (Color online) Theoretical NQR spectra for in-plane ^{63}Cu in $HgBa_2CuO_{4+\delta}$ at zero temperature and for different doping levels p.

C. Density of states and mean free path

A comparison between Eqs. (14) and (19) suggests that the hole density inhomogeneity in $HgBa_2CuO_{4+\delta}$ is pretty close to that in $La_{2-x}Sr_xCuO_4$. This seems rather surprising, given that the superconducting critical temperature in $HgBa_2CuO_{4+\delta}$ is much higher than that in $La_{2-x}Sr_xCuO_4$. Indeed, a disorder reduces the d-wave superconducting critical temperature and, based on this argument, one can expect that $La_{2-x}Sr_xCuO_4$ is "more disordered." However, one should quantify exactly what is the measure of the disorder. While the overall amplitude of the charge inhomogeneity is one possible factor, the hole mean free path is another and, in fact, more important measure of the disorder. We already noticed that the spatial charge distribution profiles induced by interstitial oxygens and Sr dopants are rather different. To quantify this difference in more detail, we calculate the quasiparticle DOS defined in the standard way

$$\rho(\epsilon) = \frac{1}{N}\sum_n \delta(\epsilon - E_n), \tag{20}$$

where N is the total number of sites, and E_n is the nth eigenenergy. Plots of the DOS in $HgBa_2CuO_{4+\delta}$ and in $La_{2-x}Sr_xCuO_4$ at doping $p = 0.16$ are shown in Figs. 8 and 9, together with the charge profiles for particular disorder realizations.The DOS has been obtained after averaging over 40 different disorder realizations. We have checked that the DOS calculated with 20 realizations of random dopant positions is practically the same as the DOS calculated with 40 realizations. This means that 40 realizations is sufficient

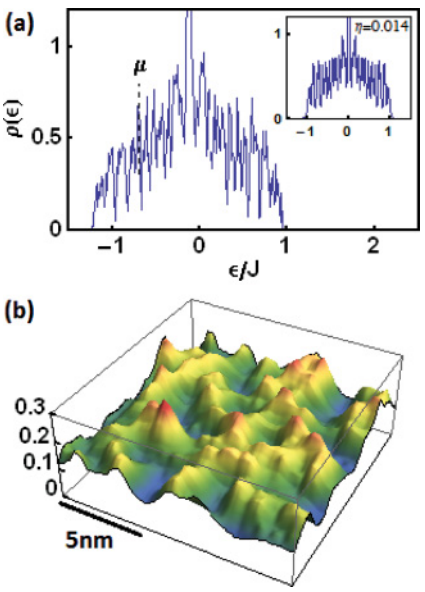

FIG. 8. (Color online) (a) DOS and (b) charge density profile in $HgBa_2CuO_{4+\delta}$ at optimal doping $p = 0.16$. Shown in the inset of panel (a) is the DOS of the homogeneous model with effective scattering rate $\eta = 0.014$.

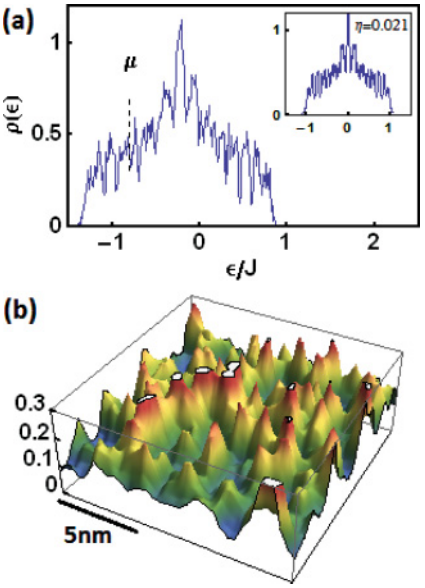

FIG. 9. (Color online) (a) DOS and (b) charge density profile in $La_{2-x}Sr_xCuO_4$ at $p = 0.16$. The inset shows the DOS of the homogeneous model with scattering rate $\eta = 0.021$.

to disregard the statistical noise. The calculated DOS exhibits pronounced oscillations. These oscillations are a byproduct of the finite size of the cluster. Maxima of the DOS correspond to degenerate states with dispersion (3) on the 36×36 torus. The oscillations must certainly disappear in the thermodynamic limit. However, oscillations have a physical meaning: They indicate that the quantum states are quite extended, with the hole mean free path l comparable with the size of the cluster used. To estimate the mean free path more accurately we use the following procedure. We consider the DOS of an ideal homogeneous system described by the Hamiltonian (2). It consists of δ functions whose positions are fixed by periodic boundary conditions. The weight of each δ function can be easily calculated for the 36×36 torus. Now we artificially broaden each δ function

$$\delta(\epsilon - \epsilon_n) \to \frac{1}{\pi} \frac{\eta}{(\epsilon - \epsilon_n)^2 + \eta^2}, \tag{21}$$

to simulate a disorder scattering. We find that the DOS of this model is very sensitive to η. Then we adjust the broadening η to reproduce (roughly) the amplitudes of the DOS oscillations obtained in our actual calculations, as shown in Figs. 8(a) and 9(a). This gives the following values of the effective broadening: $\eta = 0.014$ for $HgBa_2CuO_{4.08}$ and $\eta = 0.021$ for $La_{1.84}Sr_{0.16}CuO_4$. The mean free path of a hole at the Fermi surface can be then estimated as

$$l = v_F \tau = \frac{v_F}{2\eta}, \tag{22}$$

where $\tau = 1/2\eta$ is the collision time. At small doping $p \ll 1$, the dispersion (3) results in the Fermi velocity $v_F \approx 8t'' a_0 \sqrt{\pi p}$. Hence, at $p = 0.16$, the Fermi velocity is $v_F \approx 1.4 J a_0$. Together with the above values of η, this results in the following estimates for the hole mean free paths:

$$\begin{aligned} HgBa_2CuO_{4.08}: &\quad l \approx 50 a_0 \approx 19\,\text{nm}, \\ La_{1.84}Sr_{0.16}CuO_4: &\quad l \approx 34 a_0 \approx 13\,\text{nm}. \end{aligned} \tag{23}$$

We thus find that $La_{2-x}Sr_xCuO_4$ is indeed more disordered in the sense that it has a shorter mean free path. The different mean free paths are due to different distances from the CuO_2 plane to the Coulomb defect (interstitial oxygen versus Sr dopant) and due to different distances between Coulomb defects. In $HgBa_2CuO_{4+\delta}$, both distances are larger, therefore the Coulomb potential is smoother and hence less contributes to the large angle scattering. This difference is clearly reflected in the charge density profiles shown in Figs. 8(b) and 9(b). Overall amplitudes of the charge inhomogeneity are pretty close, but the charge distribution in $La_{2-x}Sr_xCuO_4$ is much more spiky. This gives rise to the strong scattering with large momentum transfer which is detrimental for d-wave superconductivity.

Considering the superconducting correlation length $\xi \approx 2$ nm, one finds that $l/\xi \sim 6$ in $La_{2-x}Sr_xCuO_4$ and $l/\xi \sim 10$ in $HgBa_2CuO_{4+\delta}$. One should therefore expect that the disorder suppression of superconductivity in $HgBa_2CuO_{4+\delta}$ is indeed weaker. In addition, according to our fits of the NQR data, the effective ionic dielectric constant ϵ_l in $HgBa_2CuO_{4+\delta}$, Eq. (17), is larger than that in $La_{2-x}Sr_xCuO_4$, Eq. (10). At the optimal doping $p = 0.16$, for example, $\epsilon_l(\text{LSCO}) = 60$ and $\epsilon_l(\text{HBCO}) = 150$. The larger ϵ_l in $HgBa_2CuO_{4+\delta}$ implies better screening of the Coulomb repulsion between holes and hence a smaller Coulomb pseudopotential. This may further enhance T_c of $HgBa_2CuO_{4+\delta}$ compared to that of $La_{2-x}Sr_xCuO_4$.

IV. NANOSCALE HOLE DENSITY INHOMOGENEITY IN THE SURFACE LAYER OF $Bi_2Sr_2CaCu_2O_{8+\delta}$

Recent STM experiments[3–5] have revealed large variations of pairing gaps in $Bi_2Sr_2CaCu_2O_{8+\delta}$ which are spatially correlated with the dopant oxygen density. Motivated by this observation, we now consider the charge distribution in the surface CuO_2 layer of this compound. Our purpose is to estimate the magnitude of the charge inhomogeneity induced by interstitial oxygen dopants, and see how the hole density profile is correlated with the position of these oxygens. In the present work, we do not calculate the local DOS and hence cannot address STM directly. Instead, we calculate the charge distribution similar to the previous sections, and show that the effect of interstitial oxygen on charge inhomogeneity is very significant.

As we have seen above, charge distribution profiles depend on the lattice dielectric constant whose values can be reliably obtained by fitting the NQR data. Due to lack of systematic NQR data, we cannot determine the dielectric constant of $Bi_2Sr_2CaCu_2O_{8+\delta}$ in this way. Instead, we assume that the doping dependence of the lattice dielectric constant in the bulk of $Bi_2Sr_2CaCu_2O_{8+\delta}$ is described by the same formula Eq. (17) as in $HgBa_2CuO_{4+\delta}$. This is because both compounds are doped by interstitial oxygens, which have a similar influence on lattice dynamics and dielectric screening. This adoption

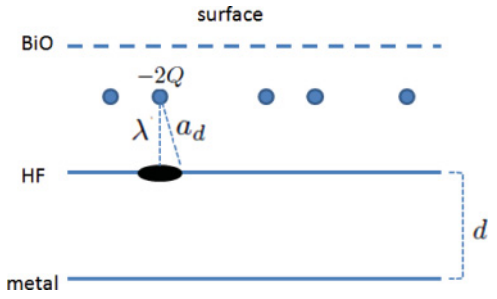

FIG. 10. (Color online) The HF model for $Bi_2Sr_2CaCu_2O_{8+\delta}$ surface. Blue dots indicate the interstitial oxygen dopants.

certainly ignores lattice structure details and should be further refined when NQR data are available. Nevertheless, we found that our results for $Bi_2Sr_2CaCu_2O_{8+\delta}$ are fairly robust within a sensible variations of the dielectric constant, and thus they should give a qualitative description of the surface charge inhomogeneity.

$Bi_2Sr_2CaCu_2O_{8+\delta}$ is a double layer compound and a schematic picture of the two surface CuO_2 layers is shown in Fig. 10. Interstitial oxygens are assumed to be located at $\lambda \approx 0.37$ nm above the CuO_2 layer, which is shown to be the most energetically favorable position.[24] We assume that the surface concentration of Coulomb defects (interstitial oxygens) is δ. They are randomly distributed and, similarly to the previous considerations, we impose again the condition that the defects never sit next to each other [i.e., the distance between the defects is always larger than $\sqrt{2}$ (in units of a_0)]. The separation between the CuO_2 layers in the double layer structure is $d = 0.33\,\text{nm} \approx 0.86$. We treat the top layer by HF approximation, and the underneath layer as a "metallic" sheet that provides screening. There are also Coulomb defects underneath of the screening layer, but they are well screened by the metallic sheet and hence do not influence the HF procedure. The hole-defect and the hole-hole interaction in the HF top layer are of the following form:

$$\mathcal{U}_{li} \to -2Q\left(\frac{1}{\sqrt{|\mathbf{R}_l - \mathbf{r}_i|^2 + a_d^2}} - \frac{1}{\sqrt{|\mathbf{R}_l - \mathbf{r}_i|^2 + (2d+\lambda)^2}}\right), \tag{24}$$

$$U_{ij} \to Q\left(\frac{1}{\sqrt{|\mathbf{r}_i - \mathbf{r}_j|^2 + a_{\text{HF}}^2}} - \frac{1}{\sqrt{|\mathbf{r}_i - \mathbf{r}_j|^2 + (2d)^2}}\right).$$

Here $a_d = \sqrt{\lambda^2 + a_{\text{ZR}}^2} \approx 1.28$, and $a_{\text{HF}} \approx \sqrt{2a_{\text{ZR}}^2} \approx 1$. Note that there is only one image charge per physical charge because there is only one screening layer. We assume that the lattice contribution to the dielectric constant in $Bi_2Sr_2CaCu_2O_{8+\delta}$ has the form of Eq. (17). On the surface, the dielectric constant is expected to be reduced to half of its value in the bulk,[16] therefore

$$\epsilon^{\text{BSCCO}} = 15(1 + 25p), \tag{25}$$

and the value of effective "charge" Q follows from Eq. (11).

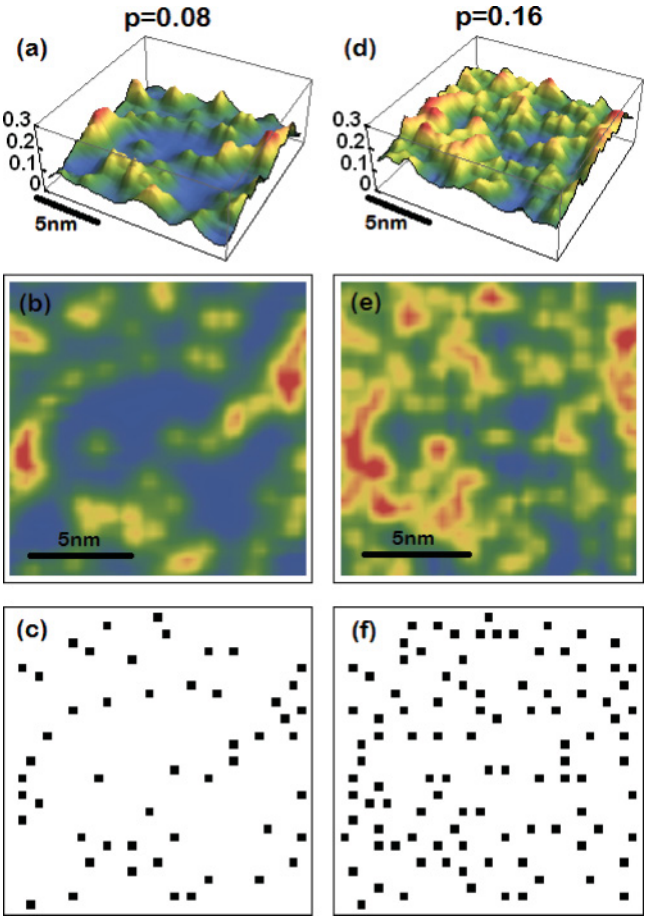

FIG. 11. (Color online) (a, d) The zero temperature hole density plots and (b, e) the hole density maps for the surface layer of $Bi_2Sr_2CaCu_2O_{8+\delta}$ for the average hole density $p = 0.08$ (left panels) and 0.16 (right panels). The lower panels (c) and (f) show positions of the oxygen dopants for the corresponding realizations of disorder. It is evident that the dopant oxygens locally increase the hole density.

Plots of the in-plane hole density for $\delta = 0.04$ ($p = 0.08$) and $\delta = 0.08$ ($p = 0.16$) are presented in Fig. 11, together with corresponding maps for these particular realizations of Coulomb defects. The plots demonstrate a large spatial variation in hole density. For the $\delta = 0.04$ case, the range of hole density modulation is about $0.03 < n_i < 0.15$, which is a very significant fluctuation, keeping in mind that the average hole density is $\langle n_i \rangle = p = 0.08$. The same strong inhomogeneity is seen in the $\delta = 0.08$ case, where the local density varies in the range roughly $0.10 < n_i < 0.23$, while average density is $\langle n_i \rangle = p = 0.16$. The density distribution curves for different doping levels are shown in Fig. 12. We stress that the precise density profiles depend on the dielectric constant which, due to lack of NQR data for $Bi_2Sr_2CaCu_2O_{8+\delta}$, is taken here in an *ad hoc* way. On a qualitative level, however, the density inhomogeneity is rather stable with respect to the value of the dielectric constant. For example, the widths of the surface density distributions plotted in Fig. 12 are only slightly larger than those obtained in the case of $HgBa_2CuO_{4+\delta}$, see Eq. (19). This is in spite of the fact that the results for $HgBa_2CuO_{4+\delta}$ have been obtained at the twice larger value of the dielectric

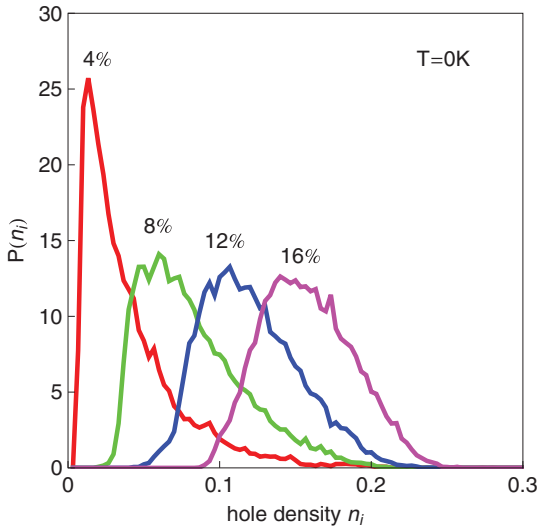

FIG. 12. (Color online) The zero temperature hole density distribution in the surface layer of $Bi_2Sr_2CaCu_2O_{8+\delta}$ at various doping levels p. Each curve is averaged over 20 realizations of disorder.

constant. Therefore, we believe that our conclusion about the strong surface charge density inhomogeneity is very reliable.

Naturally, the charge density of mobile holes is higher around areas with higher interstitial oxygen concentration. Figure 11 clearly shows this correlation. To quantify this, we define a correlation function between local hole density and dopant oxygen positions, which is analogous to the correlator introduced in Ref. 3 for the analysis of the spatial variations of the local DOS. On a discrete lattice, the hole density n_j is defined on sites of the square lattice representing the CuO_2 plane. The function f_i indicates the location of interstitial oxygens

$$f_i = \begin{cases} 1 & \text{if } i \in \text{dopant oxygen}, \\ 0 & \text{elsewhere}, \end{cases} \tag{26}$$

where i runs through points at the center of the plaquettes. The density-oxygen correlation function is then defined as

$$C_{nf}(\mathbf{R}) = \frac{1}{N}\sum_i \frac{[f_i - \overline{f}][n_{i+\mathbf{R}} - \overline{n}]}{\sqrt{A_f A_n}}, \tag{27}$$

with proper normalizations

$$A_f = \frac{1}{N}\sum_i (f_i - \overline{f})^2, \quad A_n = \frac{1}{N}\sum_j (n_j - \overline{n})^2, \tag{28}$$

where $\overline{f} = \frac{1}{N}\sum_i f_i = \delta$ and $\overline{n} = \frac{1}{N}\sum_j n_j = p$. Figure 13 shows the correlation function $C_{nf}(\mathbf{R})$ averaged over 20 disorder realizations for each doping.There is a clear positive correlation due to the Coulomb attraction to the oxygen defects. The value of the correlator at $R \to 0$ is $C \approx 0.3$–0.4 and the scale at which it goes to zero is about 10–15 Å. Interestingly, the correlator between the gap in local DOS and the interstitial oxygen position measured in STM shows the same positive correlation with very similar scales.[3] Further investigation is necessary to clarify if there is a connection

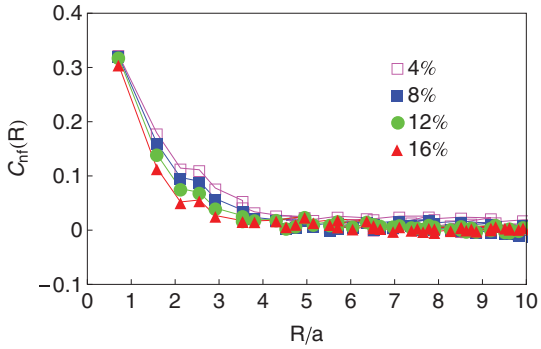

FIG. 13. (Color online) The correlation function Eq. (27) between the interstitial oxygen position and the local density of mobile holes for different values of doping p.

between these two correlators and to understand the physical reasons behind this apparent correspondence.

V. CONCLUSION

In this paper, we study the spatial distribution of doped holes in cuprates, focusing particularly on a comparison between two different physical situations: doping by a cationic substitution Sr for La as in $La_{2-x}Sr_xCuO_4$ and doping by interstitial oxygen ions as in $HgBa_2CuO_{4+\delta}$. The main results are summarized as follows.

The hole density inhomogeneity in $HgBa_2CuO_{4+\delta}$ is nearly as strong as in $La_{2-x}Sr_xCuO_4$. For example, at the optimal doping $p = 0.16$ the width of the charge density distribution is about $\Gamma_p = 0.09$, which is close to the corresponding number $\Gamma_p = 0.12$ in $La_{2-x}Sr_xCuO_4$. This conclusion is well supported by the comparison of our calculations with the existing NQR data in $HgBa_2CuO_{4+\delta}$ and $La_{2-x}Sr_xCuO_4$. In spite of the close overall amplitudes, the landscape of charge inhomogeneity in these two compounds are very different. In oxygen doped $HgBa_2CuO_{4+\delta}$, the disorder potential profiles are much smoother than that in Sr-doped $La_{2-x}Sr_xCuO_4$. Correspondingly, the hole mean free path in $HgBa_2CuO_{4+\delta}$ is larger. In other words, disorder induced scattering processes with a large momentum transfer (which are destructive for d-wave pairing) are less pronounced in oxygen doped $HgBa_2CuO_{4+\delta}$ compared to the case of $La_{2-x}Sr_xCuO_4$. In addition, the screening of the Coulomb repulsion between holes in $HgBa_2CuO_{4+\delta}$ is about two times stronger than that in $La_{2-x}Sr_xCuO_4$. In our opinion, these two reasons might explain the much higher superconducting critical temperature of oxygen doped $HgBa_2CuO_{4+\delta}$.

We found that the charge density nanoscale inhomogeneity in the surface CuO_2 layer of $Bi_2Sr_2CaCu_2O_{8+\delta}$ (the layer available for STM) is of the same magnitude as that in the bulk of $HgBa_2CuO_{4+\delta}$. As expected on physical grounds, the hole density positively correlates with the positions of interstitial dopant oxygen. Remarkably, the correlation function obtained here resembles the positive correlation between the local gap and dopant oxygens seen in the STM data. The reason for this apparent coincidence and implications of the charge inhomogeneity for the spatial variations of the pairing gaps in $Bi_2Sr_2CaCu_2O_{8+\delta}$ have to be clarified in future studies.

ACKNOWLEDGMENTS

We would like to thank J. Haase for stimulating discussions of the NQR data in cuprates and P. J. Hirschfeld, H. Alloul, M.-H. Julien, and E. Ya. Sherman for useful communications. G. Kh. thanks the School of Physics and the Gordon Godfrey fund, UNSW, for kind hospitality. Numerical calculations are done by using the facilities of the Australian National Computational Infrastructure.

[1]H. Eisaki, N. Kaneko, D. L. Feng, A. Damascelli, P. K. Mang, K. M. Shen, Z.-X. Shen, and M. Greven, Phys. Rev. B **69**, 064512 (2004).

[2]F. Rullier-Albenque, H. Alloul, F. Balakirev, and C. Proust, Europhys. Lett. **81**, 37008 (2008).

[3]K. McElroy, J. Lee, J. A. Slezak, D.-H. Lee, H. Eisaki, S. Uchida, and J. C. Davis, Science **309**, 1048 (2005).

[4]K. K. Gomes, A. N. Pasupathy, A. Pushp, S. Ono, Y. Ando, and A. Yazdani, Nature (London) **447**, 569 (2007).

[5]A. N. Pasupathy, A. Pushp, K. K. Gomes, C. V. Parker, J. Wen, Z. Xu, G. Gu, S. Ono, Y. Ando, and A. Yazdani, Science **320**, 196 (2008).

[6]P. M. Singer, A. W. Hunt, and T. Imai, Phys. Rev. Lett. **88**, 047602 (2002).

[7]D. Rybicki, J. Haase, M. Greven, G. Yu, Y. Li, Y. Cho, and X. Zhao, J. Supercond. Nov. Magn. **22**, 179 (2009).

[8]Y. Ohta, W. Koshibae, and S. Maekawa, J. Phys. Soc. Jpn. **61**, 2198 (1992).

[9]M. Mori, N. A. Shooshtary, T. Tohyama, and S. Maekawa, J. Phys. Soc. Jpn. **78**, 123704 (2009).

[10]W. Chen, G. Khaliullin, and O. P. Sushkov, Phys. Rev. B **80**, 094519 (2009).

[11]A. A. Gippius, E. V. Antipov, W. Hoffmann, and K. Lüders, Physica C **276**, 57 (1997).

[12]M.-H. Julien, M. Horvatić, P. Carretta, C. Berthier, Y. Berthier, P. Ségransan, S. M. Loureiro, and J.-J. Capponi, Physica C **268**, 197 (1996).

[13]Z. Wang, J. R. Engelbrecht, S. Wang, H. Ding, and S. H. Pan, Phys. Rev. B **65**, 064509 (2002).

[14]T. S. Nunner, B. M. Andersen, A. Melikyan, and P. J. Hirschfeld, Phys. Rev. Lett. **95**, 177003 (2005).

[15]In principle, it is possible to fit the NQR observed charge inhomogeneity even with the large Fermi surface. However, in this case one must significantly reduce the lattice dielectric constant ϵ_l. In particular, one has to take $\epsilon_l \approx 5$–6 instead of the experimentally known values $\epsilon_l \approx 30$–40.

[16]V. V. Batygin and I. N. Toptygin, *Problems in Electrodynamics* (Academic Press, London, 1978).

[17]O. P. Sushkov, G. A. Sawatzky, R. Eder, and H. Eskes, Phys. Rev. B **56**, 11769 (1997).

[18]S. E. Sebastian, N. Harrison, M. M. Altarawneh, C. H. Mielke, R. Liang, D. A. Bonn, W. N. Hardy, and G. G. Lonzarich, Proc. Natl. Acad. Sci. USA **107**, 6175 (2010).

[19]J. Singleton, C. de la Cruz, R. D. McDonald, S. Li, M. Altarawneh, P. Goddard, I. Franke, D. Rickel, C. H. Mielke, X. Yao, and P. Dai, Phys. Rev. Lett. **104**, 086403 (2010).

[20]Note that usage of the magnetic Brillouin zone notations in the t-J model does not imply that there is a long-range magnetic order. This is just a convenient way to avoid double counting of degrees of freedom related to the pseudospin, see discussion in W. Chen, O. P. Sushkov, and T. Tohyama, Phys. Rev. B **82**, 060511(R) (2010).

[21]C. Y. Chen, R. J. Birgeneau, M. A. Kastner, N. W. Preyer, and T. Thio, Phys. Rev. B **43**, 392 (1991).

[22]J. Haase, O. P. Sushkov, P. Horsch, and G. V. M. Williams, Phys. Rev. B **69**, 094504 (2004).

[23]C. Ambrosch-Draxl and E. Ya. Sherman, Phys. Rev. B **74**, 024503 (2006).

[24]Y. He, T. S. Nunner, P. J. Hirschfeld, and H.-P. Cheng, Phys. Rev. Lett. **96**, 197002 (2006).